

# The offset dependent behavior of narrow optical emission features in the Red Rectangle proto-planetary nebula<sup>★</sup>

N. Wehres<sup>1,2,★★</sup>, H. Linnartz<sup>2</sup>, H. Van Winckel<sup>3</sup>, and A. G. G. M. Tielens<sup>4,1</sup>

<sup>1</sup> Kapteyn Astronomical Institute, University of Groningen, PO Box 800, 9700 AV Groningen, The Netherlands  
e-mail: nadine.wehres@colorado.edu

<sup>2</sup> Raymond and Beverly Sackler Laboratory for Astrophysics, Leiden Observatory, Leiden University, PO Box 9513, 2300 RA Leiden, The Netherlands

<sup>3</sup> Instituut voor Sterrenkunde, K.U. Leuven, Celestijnenlaan 200B, 3000 Leuven, Belgium

<sup>4</sup> Leiden Observatory, Leiden University, PO Box 9513, 2300 RA Leiden, The Netherlands

Received 26 January 2011 / Accepted 28 June 2011

## ABSTRACT

**Context.** The Red Rectangle proto-planetary nebula provides a unique laboratory to study the physical conditions and chemical processes in stellar outflows. Snapshots of the ongoing chemical evolution are obtained by monitoring spectra as function of the offset from the central star.

**Aims.** The focus in this study is on the characterization of narrow optical emission features, that are superimposed on top of extended red emission (ERE). The primary aim is to provide a two-dimensional catalogue of these features for offsets varying from 3'' to 20'' from the central star.

**Methods.** Medium resolution emission spectra for this catalogue have been obtained through optical long-slit measurements using the New Technology Telescope (EMMI-NTT) in La Silla, Chile.

**Results.** The recorded spectra cover the range between 5550 and 6800 Å. A complete overview of the central band positions and bandwidths (*FWHMs*) is provided for both stronger (previously reported) and weaker narrow features. Only some bands are omnipresent in the nebula outflows and other bands only appear further away from the central star.

**Conclusions.** The optical emission bands show intensity variations over the nebula. We suggest that these variations reflect a spatially resolved photochemistry where larger species are photolysed, producing daughter molecules which may be the carriers of the optical emission bands.

**Key words.** astrochemistry – ISM: jets and outflows – stars: AGB and post-AGB – ISM: lines and bands

## 1. Introduction

The Red Rectangle bi-conical reflection nebula is associated with the post AGB binary star HD 44179 (Cohen et al. 1975; Van Winckel et al. 1995). The central object is an interacting binary with a ~7500 K evolved primary feeding an accretion disk around the likely unevolved secondary. This accretion disc powers a small HII region in the very center of the system (Witt et al. 2009). The star itself is visually obscured by a nearly edge on circumbinary disc (see e.g. Waelkens et al. 1996; Witt et al. 2009) and can only be seen in scattered light. The disc leads outflows into different directions, creating the appearance of an X-shaped structure (Cohen et al. 2004).

The outflows have attracted special attention as a unique laboratory providing snapshots for spatially resolved chemical processes in space. In the IR regime a series of emission features has been found between 3 and 15  $\mu\text{m}$  (see e.g. Peeters et al. 2002 and references therein) that are typical for vibrational transitions of polycyclic aromatic hydrocarbons (PAHs). Furthermore,

spectra at longer wavelengths (~20–45  $\mu\text{m}$ ) have been associated with crystalline silicates, specifically olivines ( $\text{Mg}_x\text{Fe}_{1-x}\text{SiO}_4$ ) and pyroxenes ( $\text{Mg}_x\text{Fe}_{1-x}\text{SiO}_3$ ) (Waters et al. 1998). In the optical regime the spectrum is dominated by extended red emission (ERE), a strong and broad emission feature that stretches over about 250 nm in the optical (Schmidt et al. 1980) and by broad blue luminescence in the UV (Vijh et al. 2004, 2005, 2006) that may originate from silicate nano particles or carbonaceous grains (see Duley 1985; Witt & Boroson 1990; Witt et al. 1998; Ledoux et al. 1998, 2001; Van Winckel et al. 2002; Witt & Vijh 2004). Superimposed on the ERE a chaotic pattern of narrow emission features has been found. The emission complex around 5800 Å with mainly stronger narrow emission features has been described by Schmidt & Witt (1991), Scarrott et al. (1992), Sarre et al. (1995), Van Winckel et al. (2002), Gliński & Anderson (2002), and Sharp et al. (2006). Recently, two of the weaker narrow emission bands have been attributed to C<sub>2</sub> emission features starting from rovibronically excited energy levels (Gliński et al. 2009; Wehres et al. 2010). The majority of the observed and rotationally unresolved transitions, however, has not been assigned. It is likely that these have a molecular origin, presumably transient in nature and it is possible that also rovibronically excited states play a role. Some of these narrow emission features have been proposed as the emission equivalent of some

<sup>★</sup> Based on observations collected at the European Southern Observatory, Chile. Program ID: 080.C-0814(A).

<sup>★★</sup> Current address: Center for Astrophysics and Space Astronomy, Department of Chemistry and Biochemistry, UCB 215, University of Colorado at Boulder, Boulder, CO 80309, USA.

of the well known diffuse interstellar absorption bands (DIBs) (Scarrott et al. 1992; Sarre et al. 1995; Van Winckel et al. 2002). For an opposing view see also Glinski & Anderson (2002).

The Red Rectangle proto-planetary nebula itself has been found to be carbon rich (Waters et al. 1998) and apart from the spatially resolved PAH emission in the nebula, identified molecules comprise besides  $C_2$  also CH,  $CH^+$  and CN (Balm & Jura 1992; Hobbs et al. 2004). Also oxygen rich molecules have been identified like gas phase and solid state  $CO_2$  (Waters et al. 1998), OH (Reese & Sitko 1996) and CO isotopes (Waters et al. 1998). Crystalline silicates were detected (Waters et al. 1998) and these are likely stored in the resolved stable circumbinary disc which is in Keplerian rotation around the whole inner system (Bujarrabal et al. 2005).

Variations in the spectral characteristics of the emission bands reflect different physical conditions and ongoing chemical processes in the outflows of the Red Rectangle. The intensity of the radiation field, the temperature and the densities will decrease for increasing offsets. Higher temperatures and densities will be generally in favour of a more reactive chemistry, but close to the star the stronger radiation field may also efficiently photodissociate species. In parallel, ionization and/or molecular excitation may speed up chemical processes. Further out, in the outflows, this will be less important, but species already formed are a good starting point for the formation of more complex molecules and with the absence of an intense radiation field, these may survive the harsh conditions better.

The main goal of the paper is to catalogue the narrow emission bands detected in the Red Rectangle with different offsets from the central star. A systematic and offset dependent overview of the spectral properties (band positions, widths and intensity ratios) is presented for both the stronger narrow emission features around  $5800 \text{ \AA}$  (previously studied by Schmidt & Witt 1991; Sarre et al. 1995) and the weaker narrow emission features. The latter extend work by Van Winckel et al. (2002). The second goal of this work is to derive qualitative trends that can be used as an analytical tool to visualize ongoing processes in the outflows of the Red Rectangle. The bipolar structure of the Red Rectangle is complex and spatially resolved processes are likely not covered by a single radial offset parameter. Nevertheless, as the bipolar nebula is almost in the plane of the sky, we use the angular offset as first order approximation for the radial distance from the central source. The third objective of this work is to compare the narrow emission bands with the available lists of diffuse interstellar band (DIB) positions.

This paper is organized as follows. Section 2 provides details of the observations and the data reduction procedure. The results are described in detail in Sect. 3. With this information in hand, we search in Sect. 4 for systematics in spectral changes for the observed bands at different offsets. The observed features are compared with the online DIB data as available from the catalogue by Hobbs et al. (2009). The paper concludes with a summary in Sect. 5.

## 2. Observations

The 3.5 m NTT (New Technology Telescope) at ESO, La Silla in Chile has been used to record emission spectra of the nebula for different distances from the central star HD 44179. The spectra have been obtained in the nights from February 04 and 05, 2008, using the EMMI (ESO Multi Mode Instrument) spectrograph for medium dispersion spectroscopy in long-slit spectroscopy mode. The visual magnitude of the central source HD 44179 amounts to 9.02, but this is scattered light only as the aspect angle on the

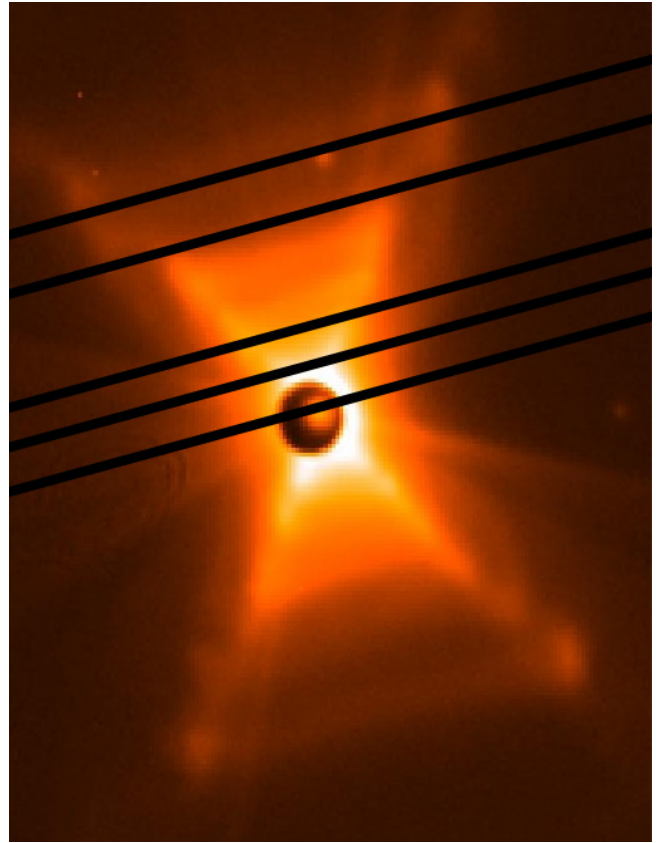


**Fig. 1.** The coronagraphic image of the Red Rectangle nebula. The image indicates the longslit settings during our observing run. Longslit settings are depicted for positions at the central star and at 3, 7, 16 and 20'' offset from HD 44179. North is up and East is to the left.

system is such that the disc blocks the direct light from the central object. For telescope settings further away from the central star the flux is decreasing fast and an adaptation of the integration time with distance was necessary. The slit was chosen to be  $1''$  in width and  $200''$  in length. These long-slit settings had a constant position angle of  $105^\circ$  east from north of HD 44179 such that the slit length was positioned parallel to the disc and tracing the outflows to the north of HD 44179 as shown in Fig. 1 (see also Van Winckel et al. 2002 Fig. 1). To increase the  $S/N$ , we collapsed the spatially resolved 2-dimensional spectra and these spectra were analysed as proxy of the nebular characteristics at that given distance to the central source. This makes it possible to compare different spectra when converted from the 2-dimensional slit spectrum into a 1-dimensional collapsed spectrum. It should be noted that this offset choice averages over different radial distances from the central star, but coincides with the distinct ladder rungs perpendicular to the nebula's outflow axis.

Different grating settings have been used (see Table 1). Grating 6 with a resolution of  $R = \lambda/\Delta\lambda = 5000$  was used for spectra recorded at the central star and for  $3''$  as well as  $7''$  offset. For larger offsets ( $16''$  and  $20''$ ) grating 7 was used that has twice the wavelength coverage and half the resolution. For each spectrum three exposures have been taken in order to correct for cosmic hits and to obtain better  $S/N$  ratios. The read-out mode for the spectra has been chosen to be slow with a binning of  $2 \times 2$  that lasted about 18 s. The pixel size of the CCD was  $15 \times 15 \mu\text{m}$ . The mean bias level was 250 ADU, the gain 1.25 electrons per ADU with a read out noise of about 3.5 ADU. The data reduction

**Table 1.** NTT-EMMI telescope settings for spectra taken at the central star and at 3, 7, 16 and 20'' offset from the central star.

Distance to HD 44179 (")	Grating	Central wavelength (Å)	Wavelength coverage (Å)	Resolution $\lambda/\Delta\lambda$	Integration time (s)	$S/N^a$ in 1-dimensional spectrum
0	6	5870	640	5000	60	229
0	6	6500	640	5000	60	268
3	6	5870	640	5000	500	207
3	6	6500	640	5000	500	149
7	6	5870	640	5000	2000	64
7	6	6500	640	5000	2000	69
16	7	6200	1300	2600	3600	34
20	7	6200	1300	2600	3600	31

**Notes.** The slit orientation is 105° east from north, perpendicular to the nebula’s symmetry axis. <sup>(a)</sup> The signal-to-noise ( $S/N$ ) was determined on a small portion of the spectrum avoiding emission and absorption lines.

was done using MIDAS in the same way as described by Wehres et al. (2010).

The standard procedure included trimming of the spectra, flat-fielding, bias subtraction, and cosmic hit cleaning. The wavelength correction was provided using He-Ar lamp spectra and the flux calibration was done using a standard star (Hiltner 600). The sky background was subtracted by extrapolating a sky-spectrum outside the region of interest. The spectra were corrected for extinction, and different integration times in order to obtain absolute fluxes. Collapsing the 2-dimensional slit spectrum resulted in a higher  $S/N$  nebular spectrum, characteristic of that given distance from the central source. The absolute  $S/N$  in the 1-dimensional spectra is indicated in Table 1 as well.

Furthermore, all spectra have been corrected for the barycentric radial velocity shift during exposure. The spectra that were recorded at the NTT are extended with a data-set taken by Van Winckel et al. (2002) at 6 and 11''. For the spectrum taken at 6'', the observations are limited to the region between 5500 and 6200 Å. Also, a so-far unpublished spectrum by Van Winckel et al. at 14'' distance has been included to the present overview.

### 3. Results

#### 3.1. An offset dependent catalogue

Details on the evolving narrow emission features are given in Fig. 2. Here, the collapsed long-slit spectra are shown for all studied offsets after subtracting the ERE, following a fit with a cubic spline function, interpolating between the different baseline points by choosing the not-a-knot endcurve condition (Behforooz 1995). We selected about 20 baseline points avoiding known narrow emission bands (Schmidt & Witt 1991; Scarrott et al. 1992; Sarre et al. 1995; Van Winckel et al. 2002; Sharp et al. 2006) as well as clear absorption features. We expect that this procedure works well here, because the focus is on the narrow emission features superimposed on the featureless ERE. The spectral parameters – central band positions and band widths ( $FWHM$ ) – of these emission features have been derived after fitting the observed bands with Gaussians. The results are summarized in Table 4. The uncertainty in this baseline is a possible source of systematic error. We have estimated the magnitude of this error by repeating this procedure many times. This systematic noise turns out to be small compared to the random noise of the observations and therefore only the latter is quoted in Table 4 as  $1\sigma$  error values.

For ease of comparison, we have subdivided each individual spectrum shown in Fig. 2 into six parts. This is illustrated for an

offset of 11'' in Fig. 3. For this offset most of the emission bands have become visible in the nebula. In this figure the Gaussian fits are included to illustrate the level of accuracy that can be obtained when fitting these features. In panels b, e and f this is clearly easier to realize than in panels a, c and d.

The fitting procedure is not trivial. Several bands are weak (but may show up stronger for other offsets, facilitating a fit), other bands consist of overlapping components, complicating unambiguous band assignments. For asymmetric bands (e.g. bands with a blue steep edge and a red degraded side) two Gaussians are used, one fitted to the steep blue side, which gives the band position, and one to the red-degraded side, which may reflect rotational substructure, similar to the procedure described in Schmidt & Witt (1991), Scarrott et al. (1992), and Sarre et al. (1995). Such unresolved bands are even more challenging to interpret for spectra recorded at offsets of 11, 14, 16 and 20'' where the selected grating has only half of the resolution. Other uncertainties that also need to be taken into account are the exact choice of the baseline and the interpretation of weaker signals, particularly in the faint parts of the nebula. It is therefore important to notice, that we specifically distinguish between bands that can be characterized unambiguously (marked with a “+” in Table 4) and bands that are visible, but with uncertain fit parameters (marked with a “?”), as well as bands (marked with a “-”) that can also be fitted choosing different sets of Gaussian parameters without substantially reducing the quality of the fit. As these bands have an increased uncertainty, we will not include these in the discussion. It should be noted that band intensities vary with offset and consequently this “+, ?, -” labeling changes as well. For 7'' offset, about 20 bands can be characterized with a label “+”. These bands will be discussed below and are indicated in bold face in Table 4.

To illustrate the spectral variations with distance to the central star, three subsections (5775–5975 Å, 5980–6180 Å and 6450–6800 Å) are shown for different offsets in Figs. 4–6 as examples of evolving emission bands. The most prominent bands in Fig. 4 (at ~5800, 5825 and 5852 Å and strong bands centered around ~6380 Å (not shown) and 6615 Å in Fig. 6) have been described before (Schmidt & Witt 1991; Scarrott et al. 1992; Sarre et al. 1995; Van Winckel et al. 2002; Sharp et al. 2006). Interesting in the present offset dependent study is the clear spectral variation of these and other bands with distance to the central star. The present study summarizes the full offset dependent behaviour of both the stronger and weaker narrow emission features (as far as these can be identified with certainty). The stronger bands have been reported in previous studies

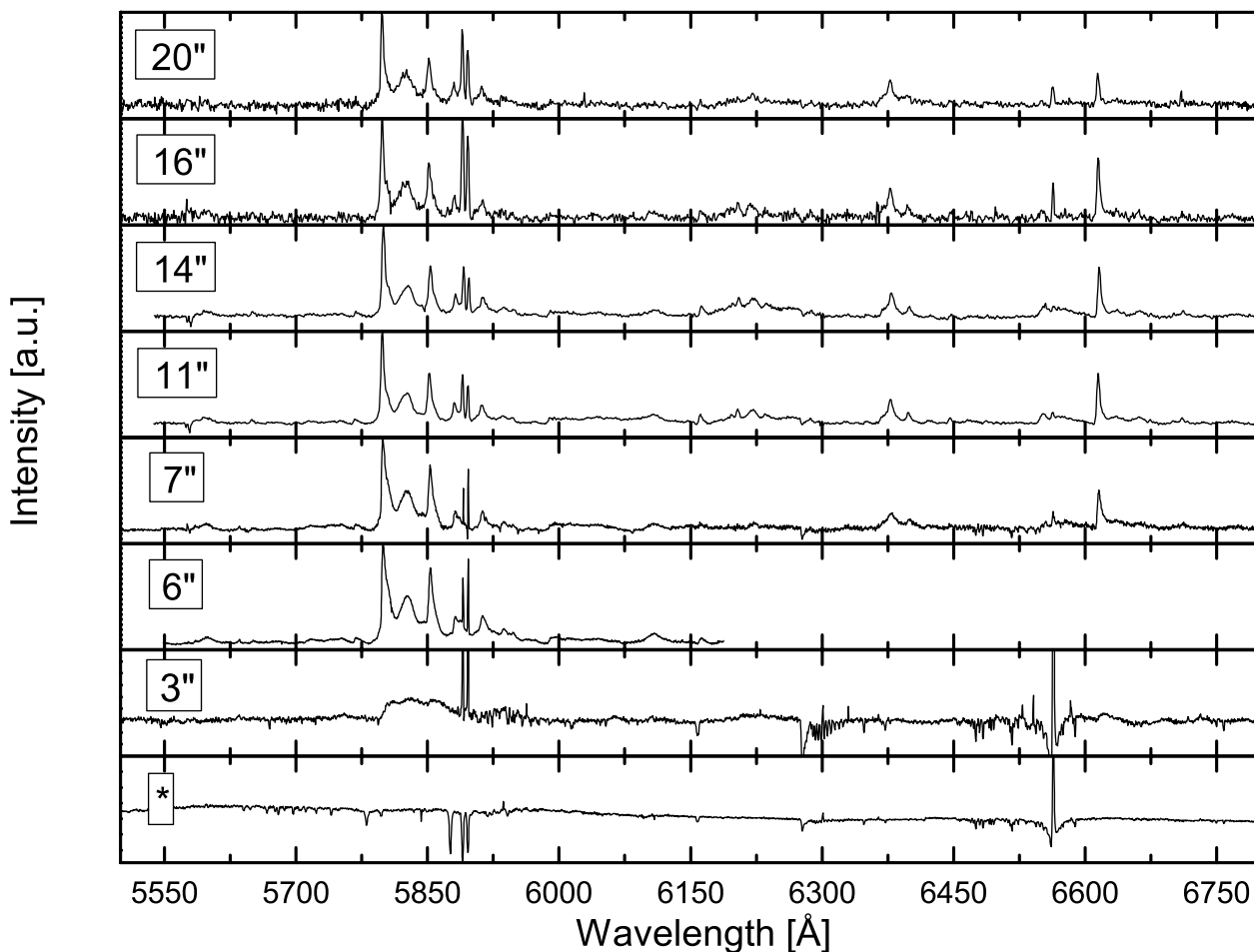


**Fig. 2.** An overview of all recorded spectra for different offsets to the central star as well as spectra taken at the central star. The ERE, if visible in the spectra, has been subtracted.

(Schmidt & Witt 1991; Scarrott et al. 1992; Sarre et al. 1995; Glinski & Nuth 1997; Van Winckel et al. 2002; Sharp et al. 2006), but not for all offsets studied here. The data given for the weaker features extend the results presented by Van Winckel et al. (2002).

A number of specific observations are reported below.

- The emission bands at  $\sim 5585$  and  $\sim 5635$  Å that recently were identified as originating from unresolved rovibronic progressions (0–1 and 1–2) within the  $d^3\Pi \rightarrow a^3\Pi$  Swan system between 3 and 7'' (Sarre 2006; Glinski et al. 2009; Wehres et al. 2010) do not reveal clear bandshifts for increasing offsets.
- The stronger emission bands in Fig. 3 (panels b, e and f), located at around  $\sim 5800$ , 5825, 5852, 6380 and 6615 Å, have been reported previously to shift towards the blue and to narrow with distance from the central star (Schmidt & Witt 1991; Scarrott et al. 1992; Sarre et al. 1995; Van Winckel et al. 2002; Sharp et al. 2006) or at least to vary with distance (Glinski & Anderson 2002). These trends are confirmed here: particularly when the bands already appear for an offset of 3'', the bandshift becomes very obvious. Many of the weaker bands presented here show a similar effect, although less pronounced.
- The spectra at 3'' are rather different from other offsets and only a few emission bands can unambiguously be characterized: the  $C_2$  lines, the Na  $D_1$  and  $D_2$  lines, the  $H\alpha$  line,

- as well as photospheric absorption lines (see Figs. 2 and 4). The photospheric atomic absorption lines that are clearly detected at 3'' are not observed for larger offset (see e.g., Fig. 4).
- Three emission features between 5990 and 6170 Å are detected, a rather unstructured band located between 5990 and 6075 Å, a pronounced emission band at around 6108 Å, and a narrow emission band at 6162 Å (Fig. 5). Most noticeable in this region is the clear relative intensity increase (1:2 to 2:1) of the 6162 Å band with respect to the 6108 Å band for 6 and 14'' distance from the exciting star. Whereas the emission band at 6108 Å is not visible at 16 and 20'', the emission band at 6162 Å can still be detected (even though it is rather weak) for an offset of 20''.
- The broad and unstructured band starting at 5990 Å has a steep incline and a broad plateau-like appearance that most likely is the result of a series of at least three blended emission bands. Several separate Gaussians have been used to reproduce this generally rather weak pattern (see Figs. 3 (panel c) and 5). This emission band is only detected for offsets between 6 and 14''.
- Four emission bands can be distinguished unambiguously around 6200–6420 Å (see Fig. 3 (panel d)) at 6196, 6204, 6222 and 6235 Å. The spectrum at 7'' only shows a first onset of these features that progress further outwards in the nebula. These bands are special, since their appearance in the nebula is only clear at larger distances from the star. Especially the

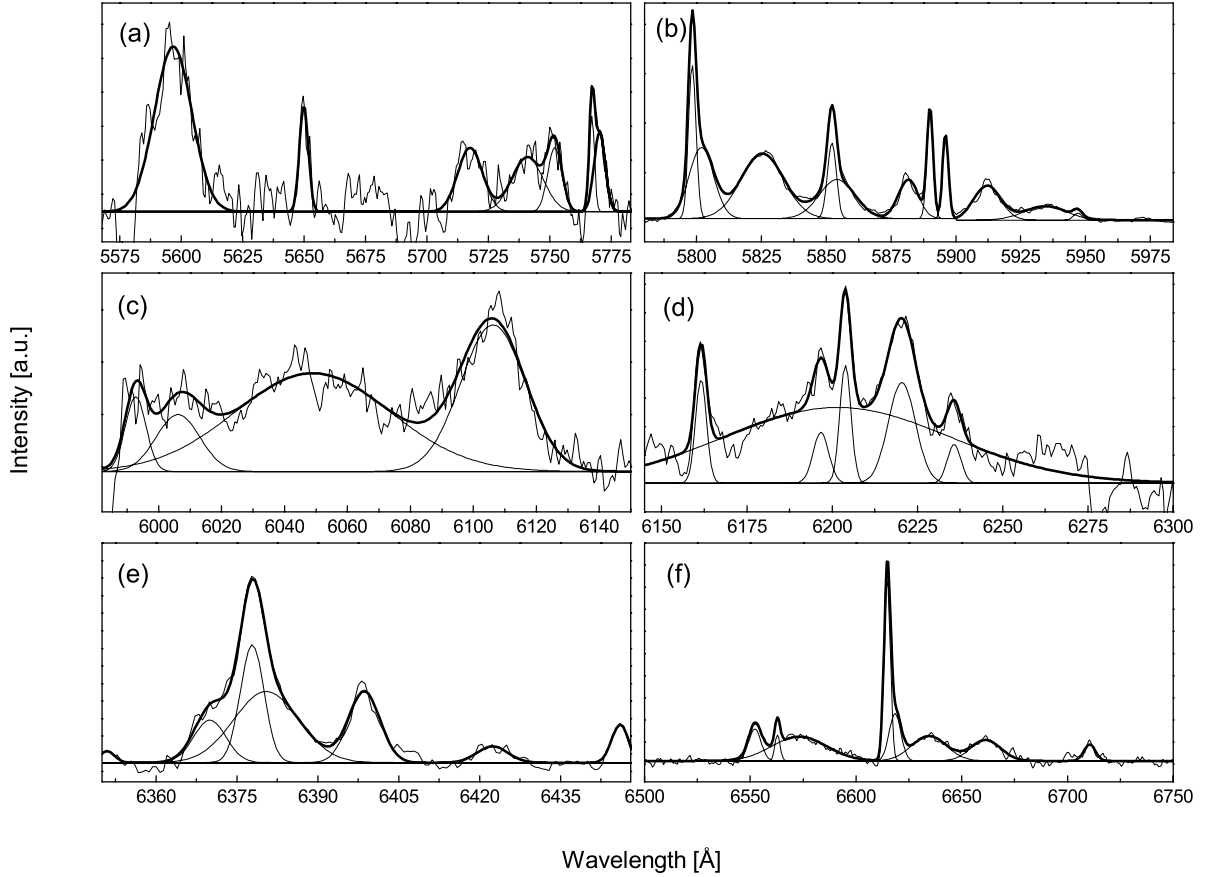


**Fig. 3.** An overview of Gaussian fits to the spectral features observed for and offset of 11", divided in six nearly equally wide wavelength regions. The sum of all fits is given as a thick black line overlaid on the observational spectrum.

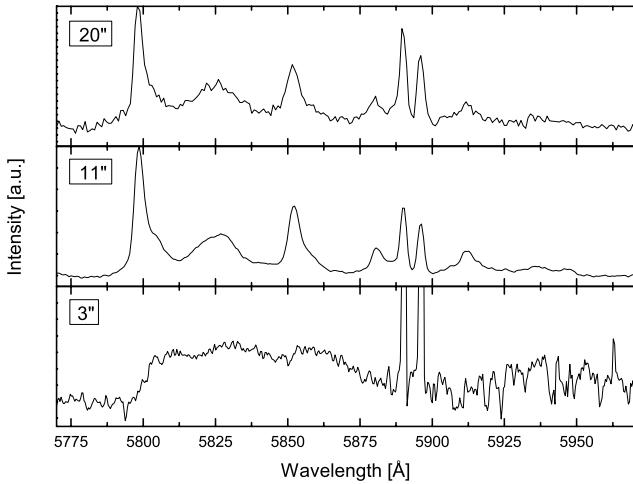


**Fig. 4.** A comparison of the narrow emission bands in the 2nd spectral range (5775–5975 Å) at 3, 11 and 20" offset to the central star. The Na doublet lines are visible at ~5890 and 5896 Å. In the 3" spectrum photospheric absorption lines are still visible, but become weaker further away from the central star. Note: for displaying purposes the y-scale is different for each panel.

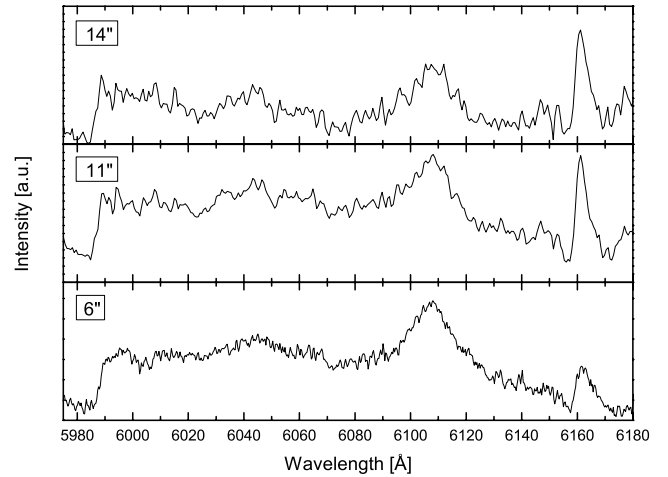


**Fig. 5.** A comparison of the narrow emission bands in the 3rd spectral range (5960–6180 Å) at 6, 11 and 14" offset towards the central star. Note: for displaying purposes the y-scale is different for each panel.

bands at 6196 and 6204 Å are detected starting from 11" onwards. The spectral lines at 6196 and 6204 Å are absent in the spectra reported by Scarrott et al. (1992), but were reported by Van Winckel et al. (2002) to start at 11".

- Other stronger narrow emission features are observed at ~6379 and 6400 Å, and weaker bands at 6420 and 6446 Å. The band at ~6379 Å has a peculiar profile showing a very narrow upper part, whereas the base of the band seems to be broadened to both sides. There is another emission band located at 5913 Å that has a similar profile. To determine the band position here, three bands, a central one, and two bands

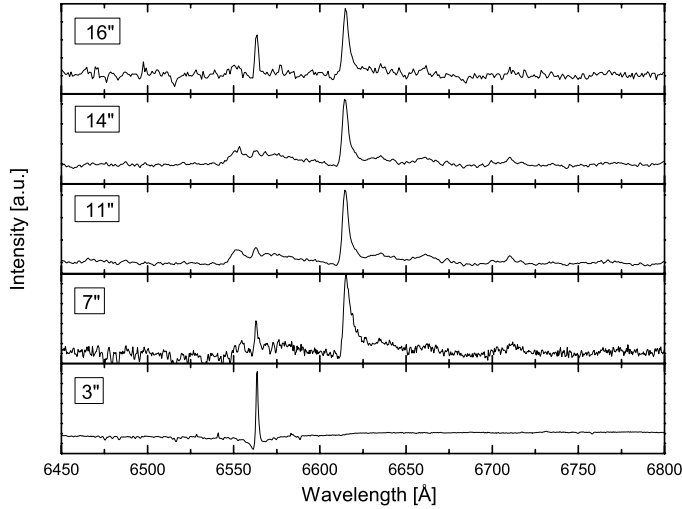


**Fig. 6.** A comparison of the narrow emission bands in the 6th spectral range (6450–6800 Å) at 3, 7, 11, 14 and 16'' offset towards the central star. Note: for displaying purposes the y-scale is different for each panel.

on either side have been fitted to give the band position as precisely as possible (see Fig. 3 (panel e)).

- The 6450 to 6800 Å range is shown in Fig. 6. An emission band at 6553 Å is close in band position and partially overlaps with the  $H\alpha$  transition at 6563 Å. It is noteworthy that the  $H\alpha$  line is strong at 3'', but then weakens fast for larger offsets. This may be expected as the  $H\alpha$  line in the Red Rectangle is mainly due to the recombination of ionized hydrogen in the innermost HII region surrounding the central star (Jura et al. 1997) and is seen mostly via scattering in the outer portions of the nebula. A stronger emission band at 6615 Å is accompanied by a series of weaker and equidistant bands (between 6633 and 6662 Å) with an approximate  $60 \text{ cm}^{-1}$  separation.

## 4. Discussion

### 4.1. Spatial behaviour of the emission bands

The shifts in band position, changes in  $FWHM$  and intensity variations of the selected “+” bands between 7 and 14'' are summarized in Fig. 7. More details on the band positions and  $FWHMs$  of the “?” and “-” bands are available from Table 4. The peak positions and  $FWHM$  of the asymmetric bands in Fig. 7 have been fitted by using multiple Gaussians. The values displayed here are not the mean values of the fitted components. Instead, we determined the peak position and  $FWHM$  by fitting a single component. The intensity ratio shown in Fig. 7 is determined for the integrated intensities of each band at 14'' relative to that at 7''.

The spectral behaviour of the bands summarized in Fig. 7 only partially exhibits similar trends, but some general features can be concluded. Most of the bands become visible at offsets beyond 3''. As from 14'' onwards, several bands decrease in intensity.

From the upper panel it can be concluded that for the larger offset (i.e., 14'') most band peak positions shift to the blue compared to 7''. The shifts amount typically to a few  $\text{cm}^{-1}$ . This is

**Table 2.** Intensity variations<sup>b</sup> of the narrow emission bands seen towards HD 44179 between 7 and 14''.

Band position in Å	7''	11''	14''
5598	0.07	0.07	0.07
<b>5651</b>	0.03	0.05	0.06
<b>5768</b>	0.05	0.05	0.06
<b>5800<sup>a</sup></b>	1.96E-14	2.71E-15	3.71E-15
<b>5826</b>	0.45	0.33	0.34
<b>5852</b>	0.70	0.54	0.55
<b>5881</b>	0.21	0.22	0.24
<b>5913</b>	0.20	0.19	0.19
5936	0.10	0.10	0.09
5990	0.07	0.07	0.06
<b>6108</b>	0.07	0.16	0.07
<b>6162</b>	0.04	0.11	0.10
6204	–	0.15	0.16
<b>6220</b>	0.05	0.11	0.14
6234	0.03	0.06	0.06
<b>6379</b>	0.10	0.26	0.26
<b>6399</b>	0.06	0.12	0.12
6446	–	0.06	0.04
<b>6553</b>	0.03	0.11	0.15
$H\alpha$	0.07	0.12	0.12
6575	0.03	0.08	0.09
<b>6615</b>	0.16	0.55	0.54
6633	0.03	0.09	0.08
6662	0.02	0.08	0.07
6710	0.03	0.06	0.08

**Notes.** Intensities of the emission bands are given relative to the band at 5800 Å. For the latter band the absolute intensity is given. <sup>(a)</sup> The absolute intensities of the 5800 Å emission band are given in  $\text{erg s}^{-1} \text{cm}^{-2} \text{arcsec}^{-2}$ . These values are close to the values reported by Schmidt & Witt (1991). <sup>(b)</sup> The uncertainties of the relative flux variations are about 0.02.

illustrated for the band at 5768 Å in Fig. 8. This is a less intense emission band that exhibits the same trends as observed previously for the stronger emission bands (Schmidt & Witt 1991; Scarrott et al. 1992; Sarre et al. 1995; Van Winckel et al. 2002; Sharp et al. 2006). Three spectra are shown for offsets of 7, 11 and 14'', respectively. The bandshift goes together with a narrowing with distance to the central star. This narrowing is also observed for other bands (Fig. 7, middle panel). The bandshift is consistent with a scenario in which a temperature effect is at play resulting in a shift of the Boltzmann maximum. As the spectra concern emission lines, care should be taken to relate these trends directly to changes of the temperature in the ground state. Nevertheless, it is likely that the observed shifts are correlated with a decrease of the temperature in the outflows. Naively, one would expect that the bandshift always goes together with a narrowing, since both are indicative for the ro-vibronic excitation temperature. However, some bands in our survey (~5651, 5913 and 6162 Å) only show a bandshift and no narrowing, which is puzzling in this respect and may be caused by multiple unresolved components. Figure 9 shows the emission band at ~5651 Å for distances at 7, 11 and 14'' exemplwise.

The lowest panel in Fig. 7 reflects the intensity variations of the emission bands between 7 and 14''. The absolute intensities at 14'' with respect to the absolute intensities of this band at 7'' are presented. The intensities for all emission bands decrease between 7 and 14'' and only make up a fraction of the intensity at 7'' (the intensity at 14'' is a few percent of the intensity at 7'').

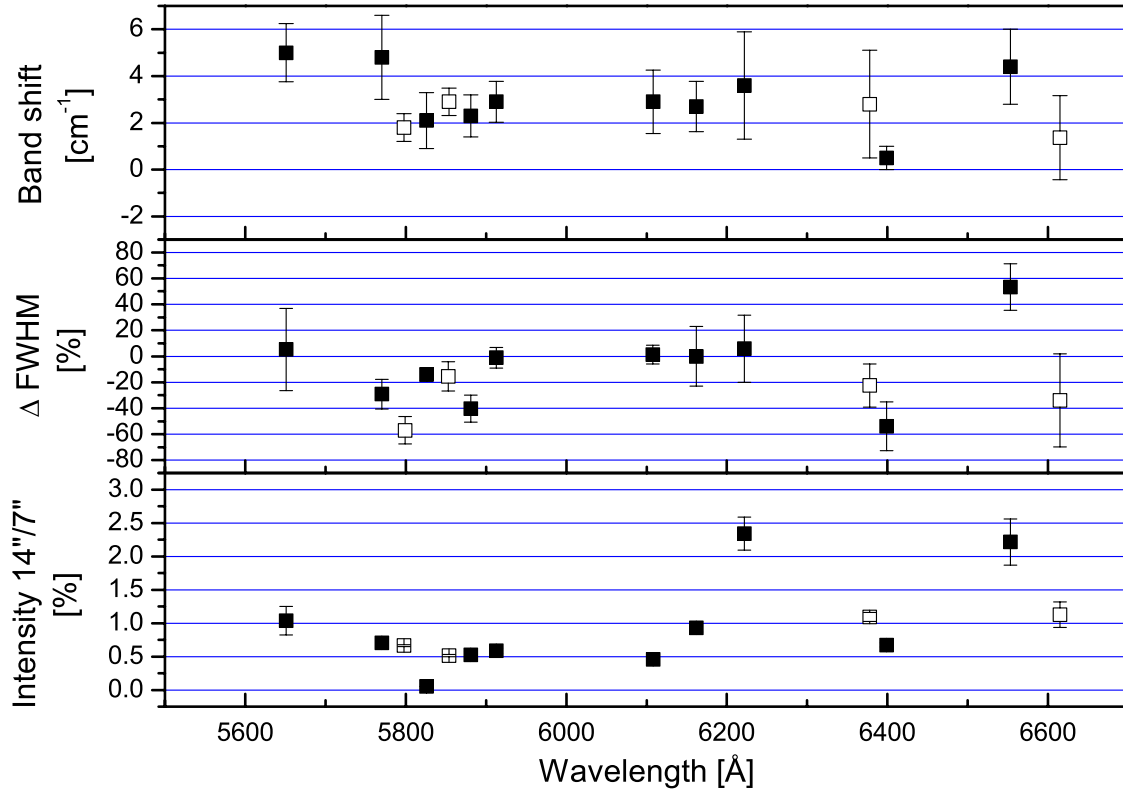


**Fig. 7.** The relative spectral changes for band peak position (*upper panel*,  $\text{cm}^{-1}$ ) and bandwidth (*FWHM*) (*middle panel*, in %) are shown. The lowest panel gives the intensity changes of the emission bands by comparing the values at 14'' and 7''. The indicated uncertainties are  $1\sigma$ -errors. The open squares include the band complex between 5800 and 5900 Å, the band at 6378 Å and the emission band at  $\sim 6615$  Å, that all have been reported previously (Schmidt & Witt 1991; Scarrott et al. 1992; Sarre et al. 1995; Van Winckel et al. 2002; Sharp et al. 2006).

**Table 3.** Summary of narrow emission features superimposed on the ERE and compared to known DIBs.

Band position [Å]	Closest detection <sup>a</sup> [']	Furthest detection <sup>a</sup> [']	Profile <sup>b</sup>	Width <sup>c</sup>	$\Delta FWHM$ 7–14''	bandshifts 7–14''	Intensity $\frac{14''}{7''}$ [%]	DIB position <sup>d</sup> [Å]	$FWHM^d$ [Å]
5651	6 (+)	14 (+)	as	n	stable	blueshift	3.4	5652.22	1.3
5767	6 (+)	14 (+)	rd	n	narrowing	blueshift	2.3	5766.98	4.50
5800	3 (+)	20 (+)	rd	n	narrowing	blueshift	2.2	5797.20	0.91
5826	3 (+)	20 (+)	s	b	narrowing	blueshift	1.7	5818.81	0.65
5852	3 (+)	20 (+)	rd	n	narrowing	blueshift	1.7	5849.88	0.93
5881	6 (+)	20 (?)	s	n	narrowing	blueshift	1.7	–	–
NaI D <sub>2</sub>	central star	20 (+)	s	n	not resolved	stable	not resolved	–	–
NaI D <sub>1</sub>	central star	20 (+)	s	n	not resolved	stable	not resolved	–	–
5913	6 (+)	20 (?)	broad wings	broad wings	stable	blueshift	1.9	5910.61	0.73
6108	6 (+)	14 (+)	s	b	stable	blueshift	1.5	6108.19	0.6
6162	6 (+)	20 (?)	s	n	stable	blueshift	3.0	6159.80	1.17
6220	7 (+)	20 (?)	s	n	stable	blueshift	7.6	6221.02	0.88
6379	7 (+)	20 (+)	broad wings	broad wings	narrowing	blueshift	3.6	6376.21	0.94
6399	7 (+)	20 (+)	s	n	narrowing	blueshift	2.2	6396.88	1.03
6553	7 (+)	20 (+)	s	n	broadening	blueshift	7.2	6553.95	0.57
H $\alpha$	central star	20 (+)	s	n	stable	stable	1.2	–	–
6615	7 (+)	20 (+)	rd	n	narrowing	blueshift	3.7	6613.70	1.08

**Notes.** <sup>(a)</sup> (+) indicates unambiguous detections, (?) indicates likely detections. <sup>(b)</sup> s = symmetric, as = asymmetric, rd = red degraded profile showing a steep blue edge. <sup>(c)</sup> Column 5 gives an indication whether a band is n = narrow or b = broad. <sup>(d)</sup> (Hobbs et al. 2009).

Two emission bands at 6220 and 6550 Å show a less steep decrease in intensity compared to the other emission bands.

Table 3 summarizes all observed data. The table gives the peak position of the emission bands in the first column. The closest and furthest offset detection of the bands are mentioned in

Cols. 2 and 3. The profiles given in Col. 4 reflect the average profile of the band over all spectra as asymmetric, symmetric or red-degraded, whereas two bands (at 5913 and 6380 Å) show broad wings on either side of the emission band. Column 5 gives an indication of the widths of the emission bands (narrow or

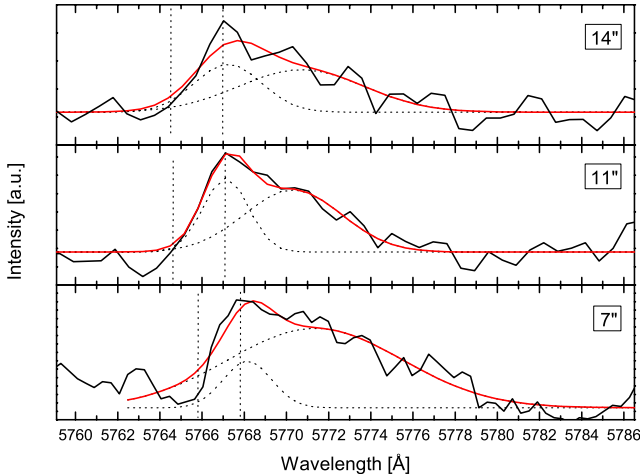


**Fig. 8.** The emission band at 5768 Å for three different offsets at 7, 11 and 14". The band was fitted (red line) using two Gaussians, indicated by the dotted lines. The bandshift is indicated with the vertical dotted lines showing the band peak position and the band onset for the three different distances.

broad) in the Red Rectangle. Columns 6–8 give a summary of the trends mentioned in Fig. 7. The main results can be summarized as follows:

- most of the bands show a symmetric profile. The most significant exceptions (at  $\sim 5800$  Å and  $\sim 6615$  Å) show red degraded profiles;
- most of the emission bands exhibit a blueshift with distance from the central star;
- most of the bands that show a blueshift also show a narrowing with distance from the central star, but not all of them. Exceptions to narrowing may be the result of multiple unresolved components;
- all of the bands decrease in absolute intensity with distance to the central star;
- most of the emission bands are observed further away than 3" from the central star.

#### 4.2. Constraints on the carriers of the emission bands

At this stage, it is good to ask the question, what constraints can be made from these measurements, particularly as only a very few of the narrow emission features have been assigned to specific carriers.

First of all, a carrier has to be reasonably abundant. In addition, the carrier molecule must be able to emit light. The UV light present around the star is capable of exciting a molecule rovibronically after which fluorescence may take place, but only when other relaxation processes (e.g., internal conversion because of a short lifetime of the excited state, or intersystem crossing) or collisional de-excitation (unlikely in the Red Rectangle outflows, Wehres et al. 2010) do not take over. Fluorescence is also enhanced if large geometry changes in the potential energy surface occur between the ground state and the excited state, since this reduces the overlap of the electronic states and consequently, fast internal conversion is not possible.

An increase or decrease of the band intensity correlates with an increasing or decreasing population density for a particular transition. In most cases intensity variations are expected to reflect a higher or lower abundance of the carrier in the nebula, but in the case of excited states, this may also be the conse-

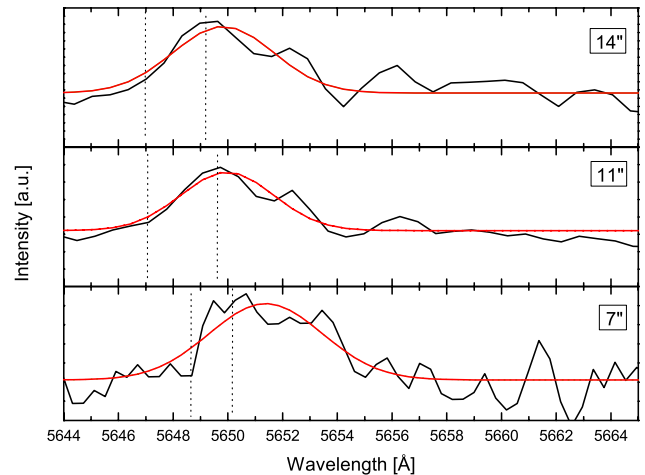


**Fig. 9.** The emission band seen at 5651 Å exhibits a blue shift with distance to the central star. A narrowing could not be determined.

quence of a change in pumping efficiency. For this reason it is helpful to look at the relative intensity variations of the emission bands. In Table 2, the relative intensities of all emission bands are given compared to the emission band at 5800 Å. The absolute intensities for the emission band at 5800 Å are indicated for the distances between 7 and 14". Here it is possible to see similar trends of the emission bands, i.e., bands that form at later stages in the nebula, decrease or increase with distance relative to the band at 5800 Å. Consequently, the normalized intensity behavior of a single emission band may give additional information on the molecular origin of a transition. A non-varying emission intensity with respect to the band at 5800 Å indicates the presence of the carrier over a wide range of conditions; the carrier may be very stable, or a pumping mechanism may be omnipresent, as can be seen e.g. for the bands between 5913, 5936 or 5990 Å, which hardly change their intensity relative to the emission band at 5800 Å.

#### 4.3. The Red Rectangle emission bands and the DIBs

The narrow emission features in the Red Rectangle have been proposed as emission equivalents of the diffuse interstellar band (DIB) absorptions. This idea is based on the fact that if the carriers of the emission features and the DIBs are identical, one might expect some fraction of their population to be in the ground state from which DIBs likely arise. Scarrott et al. (1992) and Sarre et al. (1995) argued that the carriers of certain (generally stronger) emission features in the Red Rectangle can be linked to carriers of specific DIBs and that the shifting wavelengths of the bands observed in the nebula would converge onto DIB wavelengths if measured to sufficiently large offsets from the central star of the Red Rectangle. This idea was challenged by Glinski & Anderson (2002). The present study also does not confirm this link between the Red Rectangle emission bands and the diffuse interstellar absorption bands (DIBs). Specifically, the chance of an accidental overlap is far from non-zero, given the large number of DIBs and Red Rectangle emission features in this frequency domain. This also becomes visible from Fig. 10, where the present emission data and the available DIB spectra are co-plotted. Only a few (of the stronger) bands show a partial spectral overlap, whereas *FWHM*-values generally differ considerably. Some of the emission bands have been compared to the DIBs

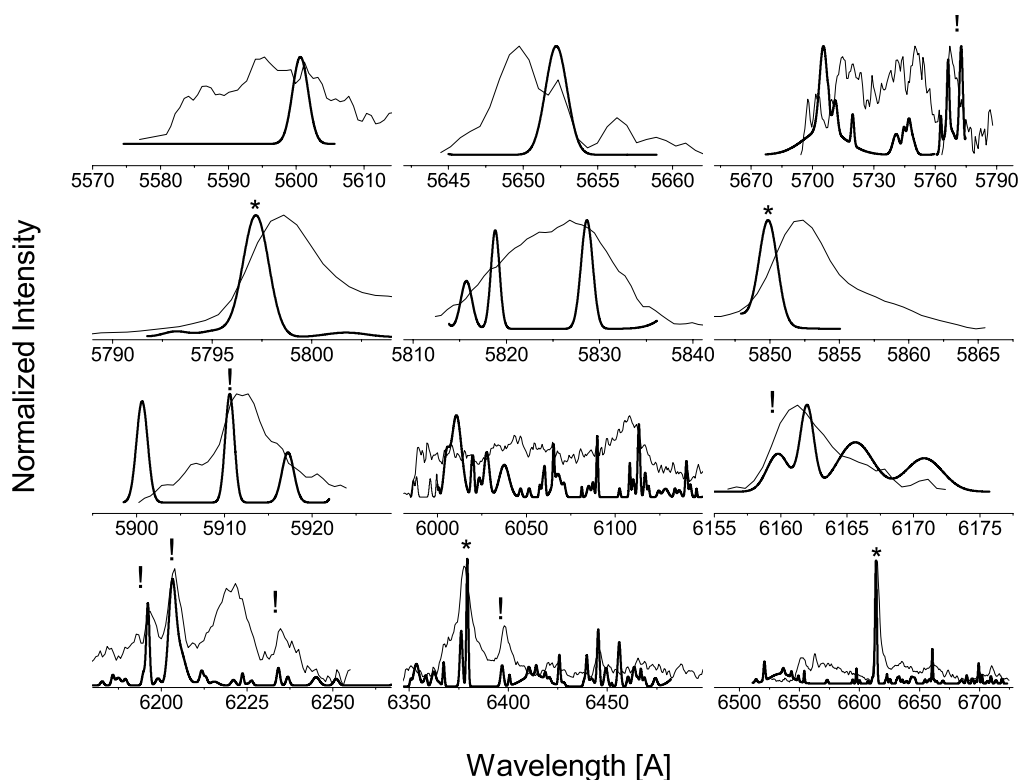


**Fig. 10.** The Red Rectangle emission spectrum taken at 11", subdivided into 12 separate plots for convenience. The emission bands of the Red Rectangle are plotted in black. Overplotted is the “inverted” DIB spectrum as thick black line Hobbs et al. (2009). Bands that show an asterisk have been compared to DIBs previously.

in the previously mentioned studies; i.e., the emission bands at  $\sim 5800$ ,  $\sim 5850$ ,  $\sim 6380$  and  $\sim 6615$  Å that have been marked with an asterisk. We can add several emission bands marked with an exclamation mark to this list:  $\sim 5767$ ,  $\sim 5913$ ,  $\sim 6162$ ,  $\sim 6196$ ,  $\sim 6204$ ,  $\sim 6240$  and at  $\sim 6399$  Å. The onsets of these emission bands are close to the onsets of reported DIBs. However, at least over the limited spatial range studied here, these emission bands show a wider *FWHM* than observed for the corresponding DIBs. In the last two columns of Table 3 the narrow emission features are compared with close lying DIBs.

#### 4.4. Chemistry

It may be instructive to recall here the behaviour of the  $C_2$  Swan-bands (Wehres et al. 2010). Specifically, the Swan-bands at 5585 and 5635 Å were detected between 3 and 7" only. The cross-section for photo-destruction, however, indicated that the molecule is rather fragile and is destroyed very efficiently in the harsh radiation field of the central star. Wehres et al. (2010) concluded that the  $C_2$  lifetime in the nebula is too short given the slow outflow velocity (Van Winckel et al. 1995; Hobbs et al. 2004; Witt et al. 2009; Wehres et al. 2010) in the nebula and a replenishment (e.g., from a PAH reservoir) is needed in order to explain the appearance of the Swan-bands in several spectra. An active photochemistry is needed to account for this e.g., the break down of PAHs in a timescale of  $10^3$ – $10^4$  years, producing  $C_2H_2$  which is then quickly photolysed to  $C_2$ . It has been suggested that such active PAH photochemistry also plays a role in the formation of hydrocarbon radicals in the ISM (Jones 2009; Pety et al. 2005).

Here we speculate that the strong emission bands seen around 5800 Å are the photoproducts of PAH molecules – observed to be present throughout the nebula – which are photolysed when they are exposed to the direct stellar light in the walls

of the outflow cones. Photolysis of the “daughter” molecules then may lead to the presence of smaller hydrocarbons (“grand-daughter” molecules), which are detected at larger distances ( $\geq 3''$ ) and may be carriers of the weaker emission bands that come and go in the outflows of the nebula. The possible correlation of the emission bands with the DIBs (Scarrott et al. 1992; Sarre et al. 1995; Van Winckel et al. 2002) – and given the discrepancy in the *FWHMs* – would imply then that the carriers of the DIBs in diffuse interstellar clouds are also due to smaller hydrocarbon species. This would be in line with the recent possible identification of the  $\lambda 5450$  DIB with the  $C_3H_2$  radical (Maier et al. 2011), following a previous study by (Linnartz et al. 2010). This assignment to  $C_3H_2$  is currently under debate (Oka & McCall 2011; Krelowski et al. 2011) and needs to be proven correct or wrong.

We also note that the  $60\text{ cm}^{-1}$  spacing in the 6615 Å band – if interpreted as a vibrational progression – is indicative of a rather small hydrocarbon chain.  $C_3$  itself for example has low lying bending modes of about  $60\text{ cm}^{-1}$ . While the evidence for  $C_3$  is not controversial (Glinski & Nuth 1997) lower vibrational modes of larger carbon chains shift generally with the size of the chain and a  $60\text{ cm}^{-1}$  shift would correspond to a size of 7 to 8 carbon atoms.

## 5. Conclusions

The offset dependent spectra for the Red Rectangle protoplanetary nebula are presented for offsets at 3, 6, 7, 11, 14, 16 and 20" distance from the central star. The spectra show that spectral features change as function of distance:

- Only some of the emission bands are omnipresent and are found at 3" offset, and most bands become visible from 7" onwards.



- The majority of the bands that can unambiguously be fitted, shifts a few  $\text{cm}^{-1}$  to the blue for larger offsets.
- Several of these bands simultaneously become narrower.

As the spectra concern emission lines, care has to be taken to directly relate these observations to e.g. temperature changes in the ground state, but it is likely that shifts and narrowing are due to a varying temperature in the outflows.

Several bands are observed that are clearly indicative for ongoing chemical and physical processes in the outflows of the Red Rectangle: some bands appear others vanish. Following the interpretation of the  $\text{C}_2$  Swan-bands, we interpret this as reflecting a chemical process (a molecule is formed or destroyed) and as such the emission bands are a good visualization of an ongoing active (photo)chemistry in the outflows of the Red Rectangle. A link with DIBs could not be confirmed.

*Acknowledgements.* N.W. acknowledges the financial support provided through the European Community's Human Potential Program under contract, MCRTN 512302, The Molecular Universe. We also acknowledge the financial support provided through the advanced ERC-grant 246976, Studies of interstellar PAHs at Leiden Observatory. This work was supported by the Netherlands Research School For Astronomy (Nederlandse Onderzoeksschool voor Astronomie) NOVA and the Sackler Laboratory for Astrophysics at Leiden University. We also would like to thank ESO and the staff at La Silla for assistance and support during the observations.

## References

- Balm, S. P., & Jura, M. 1992, *A&A*, 261, L25  
 Behforooz, G. H. 1995, *Appl. Math. Comput.*, 72, 219  
 Bujarrabal, V., Castro-Carrizo, A., Alcolea, J., & Neri, R. 2005, *A&A*, 441, 1031  
 Cohen, M., Anderson, C. M., Cowley, A., et al. 1975, *ApJ*, 196, 179  
 Cohen, M., Van Winckel, H., Bond, H. E., & Gull, T. R. 2004, *AJ*, 127, 2362  
 Duley, W. W. 1985, *MNRAS*, 215, 259  
 Glinski, R. J., & Anderson, C. M. 2002, *MNRAS*, 332, L17  
 Glinski, R. J., & Nuth, III, J. A. 1997, *Ap&SS*, 249, 143  
 Glinski, R. J., Michaels, P. D., Anderson, C. M., et al. 2009, *Ap&SS*, 323, 337  
 Hobbs, L. M., Thorburn, J. A., Oka, T., et al. 2004, *ApJ*, 615, 947  
 Hobbs, L. M., York, D. G., Thorburn, J. A., et al. 2009, *ApJ*, 705, 32  
 Jones, A. P. 2009, in *ASP Conf. Ser.* 414, ed. T. Henning, E. Grün, & J. Steinacker, 473  
 Jura, M., Turner, J., & Balm, S. P. 1997, *ApJ*, 474, 741  
 Krelowski, J., Galazutdinov, G., & Kolos, R. 2011, *ApJ*, submitted  
 Ledoux, G., Ehbrecht, M., Guillois, O., et al. 1998, *A&A*, 333, L39  
 Ledoux, G., Guillois, O., Huisken, F., et al. 2001, *A&A*, 377, 707  
 Linnartz, H., Wehres, N., van Winckel, H., et al. 2010, *A&A*, 511, L3  
 Maier, J. P., Walker, G. A. H., Bohlender, D. A., et al. 2011, *ApJ*, 726, 41  
 Oka, T., & McCall, B. J. 2011, *Science*, 331, 293  
 Peeters, E., Hony, S., Van Kerckhoven, C., et al. 2002, *A&A*, 390, 1089  
 Pety, J., Teyssier, D., Fossé, D., et al. 2005, *A&A*, 435, 885  
 Reese, M. D., & Sitko, M. L. 1996, *ApJ*, 467, L105  
 Sarre, P. J. 2006, *J. Mol. Spectrosc.*, 238, 1  
 Scarrott, S. M., Watkin, S., Miles, J. R., & Sarre, P. J. 1992, *MNRAS*, 255, 11P  
 Sarre, P. J., Miles, J. R., & Scarrott, S. M. 1995, *Science*, 269, 674  
 Schmidt, G. D., & Witt, A. N. 1991, *ApJ*, 383, 698  
 Schmidt, G. D., Cohen, M., & Margon, B. 1980, *ApJ*, 239, L133  
 Sharp, R. G., Reilly, N. J., Kable, S. H., & Schmidt, T. W. 2006, *ApJ*, 639, 194  
 Van Winckel, H., Waelkens, C., & Waters, L. B. F. M. 1995, *A&A*, 293, L25  
 Van Winckel, H., Cohen, M., & Gull, T. R. 2002, *A&A*, 390, 147  
 Vijn, U. P., Witt, A. N., & Gordon, K. D. 2004, *ApJ*, 606, L65  
 Vijn, U. P., Witt, A. N., & Gordon, K. D. 2005, *ApJ*, 619, 368  
 Vijn, U. P., Witt, A. N., York, D. G., et al. 2006, *ApJ*, 653, 1336  
 Waelkens, C., Van Winckel, H., Waters, L. B. F. M., & Bakker, E. J. 1996, *A&A*, 314, L17  
 Waters, L. B. F. M., Cami, J., de Jong, T., et al. 1998, *Nature*, 391, 868  
 Wehres, N., Romanzin, C., Linnartz, H., van Winckel, H., & Tielens, A. G. G. M. 2010, *A&A*, 518, A36  
 Witt, A. N., & Boroson, T. A. 1990, *ApJ*, 355, 182  
 Witt, A. N., & Vijn, U. P. 2004, in *Astrophysics of Dust*, ed. A. N. Witt, G. C. Clayton, & B. T. Draine, *ASP Conf. Ser.*, 309, 115  
 Witt, A. N., Gordon, K. D., & Furton, D. G. 1998, *ApJ*, 501, L111  
 Witt, A. N., Vijn, U. P., Hobbs, L. M., et al. 2009, *ApJ*, 693, 1946